The Role of Al3+-Based Aqueous Electrolytes in the Charge Storage Mechanism of MnOx Cathodes

Véronique Balland, Mickaël Mateos, Arvinder Singh, Kenneth D Harris, Christel Laberty- Robert, Benoît Limoges

The role of Al^{3+}-based aqueous electrolytes in the charge storage mechanism of MnO_x cathodes

Véronique Balland,[†,] Mickaël Mateos,[†] Arvinder Singh,[¤] Kenneth D. Harris,[‡,§] Christel Laberty-Robert,[¤] Benoît Limoges[†,*]*

Dr. V. Balland, Dr. M. Mateos, Dr. A. Singh, Dr. K.D. Harris, Pr. C. Laberty-Robert, Dr. B. Limoges

† Université de Paris, Laboratoire d'Electrochimie Moléculaire, UMR CNRS 7591, F-75013 Paris, France.

¤ Laboratoire de Chimie de la Matière Condensée de Paris, Sorbonne Université, Paris F-75005, France

‡ National Research Council Canada, Nanotechnology Research Centre, Edmonton, Alberta, T6G 2M9, Canada

§ Department of Mechanical Engineering, University of Alberta, Edmonton, Alberta, T6G 2V4, Canada

E-mail: veronique.balland@u-paris.fr, limoges@u-paris.fr,

Keywords: aqueous battery, zinc battery, MnO_2, conversion mechanism, aluminium-ion, proton insertion

Abstract

Rechargeable aqueous aluminium batteries are the subject of growing interest, however, the charge storage mechanisms at manganese oxide-based cathodes remain poorly understood. In essense, every study proposes a different mechanism. Here, we use an *in situ* spectroelectrochemical methodology to unambiguously demonstrate that reversible proton-coupled MnO_2-to-Mn^{2+} conversion is the main charge storage mechanism occurring at MnO_2 cathodes for a range of slightly acidic Al^{3+}-based aqueous electrolytes, with the Al^{3+} hexaaquo complex playing the key role of proton donor. In Zn/MnO_2 assemblies, this mechanism is associated with high gravimetric capacities and discharge potentials, up to 560 $mAh \cdot g^{-1}$ and 1.65 V respectively, attractive efficiencies (*CE* > 99.5 % and *EE* > 82%) and excellent cyclability (almost 100% capacity retention over 1 400 cycles at 2 $A \cdot g^{-1}$). Finally, we conducted a critical analysis of the data previously published on MnO_x cathodes in Al^{3+}-based aqueous electrolytes to conclude on a universal charge storage mechanism, *i.e.*, the reversible electrodissolution/electrodeposition of MnO_2.

1. Introduction

Insertion of earth-abundant multivalent (MV) metal cations (*e.g.*, Mg^{2+}, Zn^{2+} and Al^{3+}) into host electrode materials is currently the subject of much attention due to the promising potential to go "beyond lithium". This is especially true with regard to the development of new insertion-based rechargeable aqueous batteries, which are currently under intensive study due to cost, safety and eco-sustainability considerations.[1,2] However, the real ability of multivalent cations to reversibly insert into redox-active materials, especially metal oxide-based hosts, is still uncertain.[3] Indeed, it has long been believed that the strong electrostatic interaction of MV cations with metal oxide lattices considerably hinders solid-state diffusivity,[4] leading to low electrochemical activity even in the presence of a strong thermodynamic driving force. Moreover, the high solvation energy of MV cations, especially in water, is an additional insertion barrier, adding to the difficulties of MV-ion insertion. Despite all of this, numerous recent works report the reversible insertion of MV cations into metal oxides in the presence of water, and under these conditions, they demonstrate electrochemical performances much better than in pure organic electrolytes.[5–7] However, a growing number of recent studies propose that the attractive performances observed with aqueous MV-ion batteries result from the reversible insertion of protons into the host electrode rather than MV cations. This has been evidenced in particular for VO_2,[8] V_2O_5,[9] $Na_3V_2(PO_4)_2F_3$,[10] and TiO_2[11] electrodes cycled in either mild acidic Zn^{2+}- or Al^{3+}-based aqueous electrolytes. Moreover, in our previous work on TiO_2, we demonstrated that the source of protons in mild aqueous electrolytes was neither water nor H_3O^+, but the hexaaquo MV complexes (*e.g.*, $[Zn(H_2O)_6]^{2+}$, $[Al(H_2O)_6]^{3+}$) which spontaneously form in water and become weak Brønsted acids.[11] Additionally, we have shown that the hexaaquo cations $[Zn(H_2O)_6]^{2+}$ and $[Mn(H_2O)_6]^{2+}$, commonly present in the aqueous electrolytes of Zn/MnO_2

batteries, can act as proton sources to trigger the electrodissolution of MnO_2 into Mn^{2+}.[12] These studies underline the crucial, but little-known role played by the weak acidity of hydrated MV ions on the charge storage mechanisms at metal oxide electrodes. An illustration is provided by the trivalent Al^{3+} cation, which has recently been promoted for "rechargeable aqueous aluminium batteries", wherein an aluminium (or zinc) anode is paired with a MnO_x cathode in an Al^{3+}-based aqueous electrolyte.[13–18] A collective issue with these works, however, is the disparate variety of charge storage mechanisms and cathode compositions that are proposed. Indeed, some works suggest the reversible insertion of MV cations (Al^{3+} or Zn^{2+}) into either the pristine K_xMnO_2 phase[16] or an Al_xMnO_2 phase generated from a solid Mn_3O_4,[14] MnO[18] or MnO_2[17] precursor. Other reports assume a reversible conversion process, either solid-solid (*i.e.*, MnO_2-to-Mn_3O_4)[13] or solid-solute (*i.e.*, Al_xMnO_2-to-Mn^{2+}),[15] but without clearly describing the role and source of protons, which is a major mechanistical issue.

In light of the numerous and contradictory mechanistic propositions, our objective with the present work is to decipher the exact role of Al^{3+} ions in the reversible charge storage mechanism of MnO_x cathodes immersed in Al^{3+}-based aqueous electrolytes. As we will see, our results unambiguously support a mechanism based on the reversible proton-coupled electrodissolution of solid MnO_x materials into soluble Mn^{2+} ions, wherein the hexaaquo complex $[Al(H_2O)_6]^{3+}$ plays the key role of proton donor over a wide range of slightly acidic Al^{3+}-based electrolyte compositions. Such a mechanism challenges the previously-reported charge storage mechanisms which are critically reviewed here.[13–18]

2. Results and Discussion

MnO_x cathodes were prepared as previously described[19,20] by anodic electrodeposition of the active material (in a buffered pH 5 electrolyte containing 0.1 M $MnCl_2$) into the pore structure of two different types of 3D conductive scaffolds (see Experimental Section in Supporting Information), *i.e.* 3D transparent electrodes made of a 1 µm-thick nanostructured ITO film deposited by glancing angle deposition (GLAD) over a flat commercial ITO-coated glass substrate[21] and 3D assemblies of self-standing electrospun carbon nanofibers (*i.e.*, 360 µm-thick CNFs with an average fiber diameter of 127 ± 47 nm).[20] The main interest of the MnO_x-loaded 3D transparent ITO electrodes is that they offer the possibility to quantitatively monitor, by *in operando* UV-visible spectroelectrochemistry, the fate of MnO_x during galvanostatic cycles (see **Scheme 1** depicting the three-electrode setup).[19] For such a purpose, the GLAD-ITO electrodes were loaded by systematically applying a deposited charge of 100 $mC \cdot cm^{-2}$. This results in the deposition of 48 ± 1 $\mu g \cdot cm^{-2}$ of MnO_x within the GLAD-ITO film mesoporosity. The XRD analysis confirmed the amorphous state of MnO_x while the ICP and XPS analyses converged on an average Mn oxidation state (AOS) of 3.86.[19] The deposited film thus corresponds to $MnO_{1.93}$ but, for the sake of simplicity, we kept the notation "MnO_2" in the following. This AOS value of 3.86 also allows us to calculate a theoretical maximal gravimetric capacity of 574 $mA \cdot h/g_{MnO2}$.

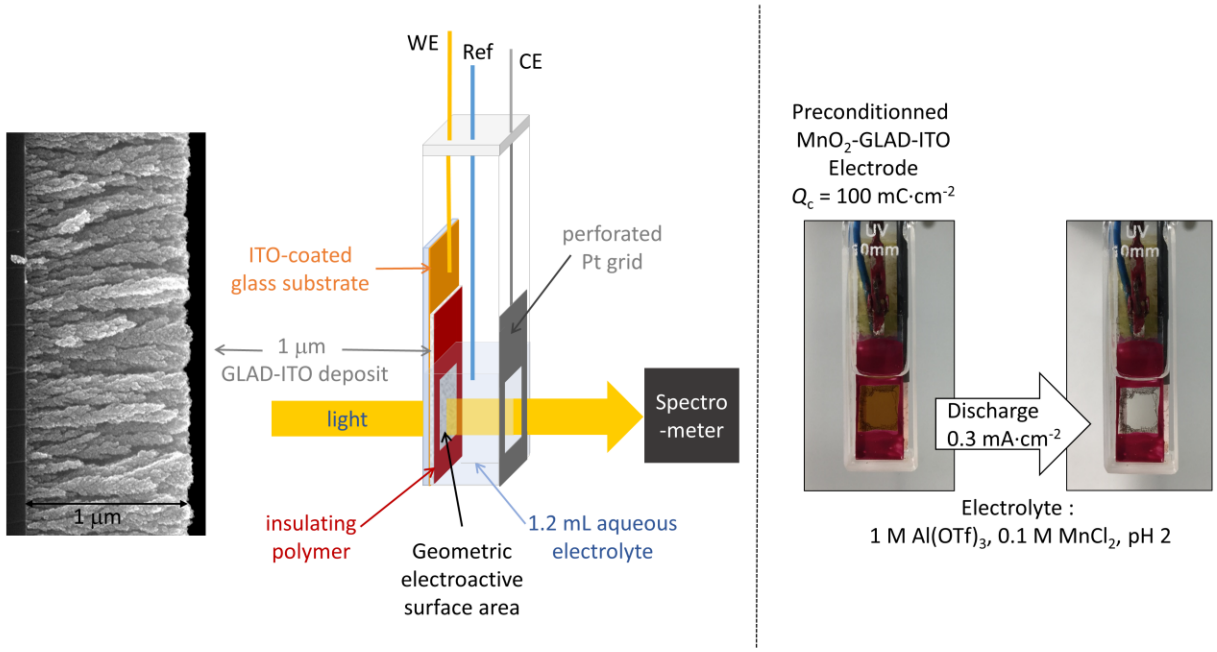

Scheme 1. Left: schematic of the *in operando* spectroelectrochemical setup used to monitor a MnO_2-loaded GLAD-ITO electrode (made of a 1-µm thick transparent nanostructured film of GLAD-ITO). Right: photographs of the spectroelectrochemical cell taken at the beginning and end of a galvanostatic discharge experiment performed at a GLAD-ITO electrode loaded *ex situ*.

To scale-up to a format closer to a laboratory battery, we relied on a Zn/MnO_2 Swagelock cell consisting of a zinc foil and a self-supporting spun carbon nanofiber mat coated with MnO_2.[20] On account of the much larger electroactive surface of the CNFs as compared to the GLAD-ITO electrode, the electrodeposition time was adjusted to achieve a 1 C·cm^{-2} charge, equivalent to the deposition of 0.5 mg·cm^{-2} MnO_2.

2.1. *In-operando* spectroelectrochemical analysis of the charge storage mechanism

The electrochemical reactivity of the MnO_2-GLAD-ITO electrodes was first examined with and without Al^{3+} in different aqueous electrolytes adjusted to pH 2.0 (see Table S1 for

chemical compositions). The spectroelectrochemical data associated with the first galvanostatic discharges are given in **Figure 1** (A and B).

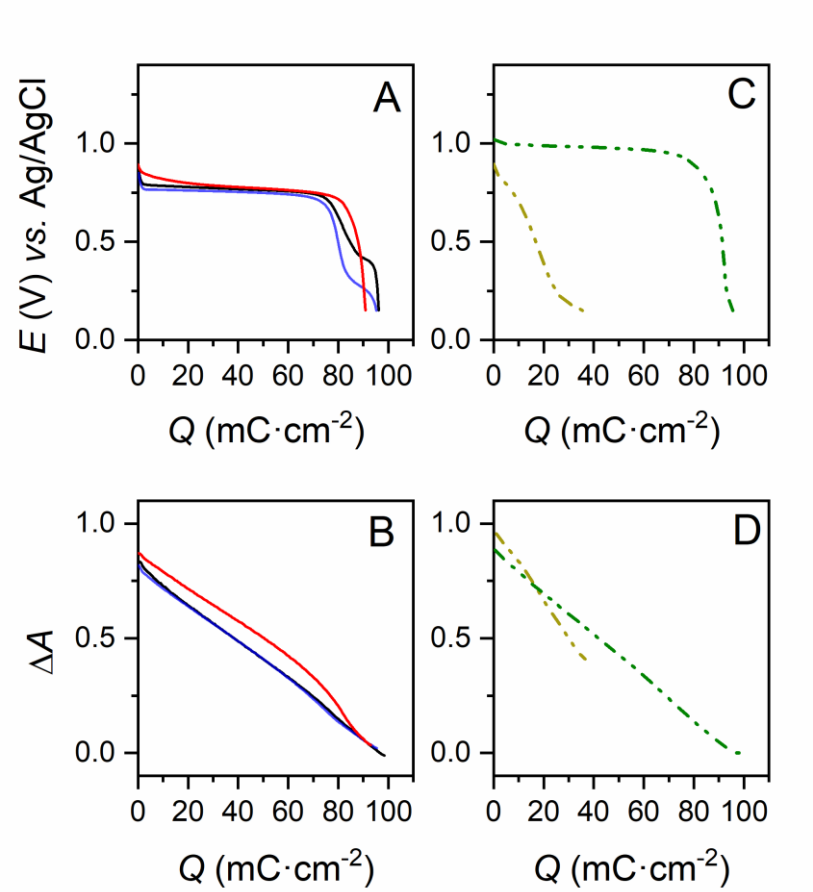

Figure 1. *In operando* spectroelectrochemical characterization of the first discharge of MnO_2-GLAD-ITO electrodes in different aqueous electrolytes (all adjusted to pH 2.0 except for dashed olive data corresponding to pH 1.0). (A, C) Galvanostatic curves (rate: 0.3 $mA \cdot cm^{-2}$) and (B, D) absorbance variations concomitantly recorded at MnO_2-GLAD-ITO electrodes (loaded *ex situ* with a deposited charge of 100 $mC \cdot cm^2$) immersed in the following electrolytes: (red) 1 M acetic acid + 0.1 M $MnCl_2$ + 2 M KCl, (blue) 1 M $Al(OTf)_3$ + 0.1 M $MnCl_2$, (plain black) 1 M $AlCl_3$ + 0.1 M $MnCl_2$, (dashed lines) 2 M KCl + 0.1 M $MnCl_2$ adjusted to (dark yellow) pH 2.0 or (olive) pH 1.0.

In a 1 M acetic acid electrolyte (along with 0.1 M $MnCl_2$) adjusted to pH 2.0, the galvanostatic discharge curve is characterized by a well-defined single plateau (red line in Fig. 1A), leading to an areal discharge capacity (C_d) of 92 $mC \cdot cm^{-2}$ (Table S1), close to the *ex situ* deposited charge of 100 $mC \cdot cm^{-2}$ (thus corresponding a Coulombic efficiency of *CE* = 92%). Concomitantly, the absorbance of the electrode decreases almost linearly to near zero (red line in Fig. 1B), which signals the near complete electrodissolution of MnO_2. This is further confirmed by the low m_{MnO_2} value obtained for the discharged electrode (Table S1), indicating that only ~4% of the initially electrodeposited Mn remains on the electrode. As a result, the discharge gravimetric capacity is 530 $mA \cdot h \cdot g^{-1}$, close to the theoretical value. Obviously, the presence of 0.1 M $MnCl_2$ in the electrolyte does not impede or inhibit the MnO_2 electrodissolution, contrary to what has been suggested in previous works.[17,22]

These observations are in line with those we have recently reported[19] in a 1 M acetate buffer of pH 5, and they support the following proton-coupled electron transfer reaction in which acetic acid is involved as a proton donor:

$$Mn^{IV}O_2 + 4\ CH_3COOH + 4\ H_2O + 2\ e^- \rightarrow [Mn^{II}(H_2O)_6]^{2+} + 4\ CH_3COO^- \quad (1)$$

It is important to point out here that this global equation is associated with a complex mechanism involving multiple elementary steps. An initial proton-coupled electron transfer reaction probably forms the transient MnOOH species, which is then followed either by a second fast multi-proton-coupled electron transfer reaction leading to the soluble Mn^{2+} aqua complex, or by a disproportionation reaction between two Mn^{III} species into soluble Mn^{2+} and insoluble Mn^{IV} species (thus agreeing with the thermodynamics of the system, *i.e.* $E^{0'}_{MnO_2/MnOOH} < E^{0'}_{MnOOH/Mn^{2+}}$ at pH 2,[23] as well as the single 2-electrons discharge plateau). To the complexity of this mechanism must also be added the facts that it is coupled with nucleation and growth kinetics

that can potentiallly control the rate of MnO_2 electrodissolution, and also with charge transport that probably propagates through the film by electron hoping and/or conduction band charge transport.[24,25] Whatever the mechanism, the global reaction 1 under thermodynamic equilibrium conditions translates into the following Nernst equation (an equation which thus governs the equilibrium potential of the charge/discharge curves):

$$E = E^0_{MnO_2/Mn^{2+}} - 0.12 \times pH - 0.03 \times \log\left(a_{Mn^{2+}}\right) \quad (2)$$

where $E^0_{MnO_2/Mn^{2+}}$ is the standard potential of the MnO_2/Mn^{2+} redox couple (*i.e.*, 1.15 V *vs.* Ag/AgCl),[12] $a_{Mn^{2+}}$ is the activity of soluble Mn^{2+} ions, and the pH corresponds to the local value at the MnO_2/electrolyte interface. The higher value reported here for the half-discharge potential (E_d= 0.74 V *vs.* Ag/AgCl) as compared to the value we previously obtained in a 1 M acetate buffer of pH 5 (E_d = 0.50 V *vs.* Ag/AgCl)[12,19] is thus fully consistent with the lower pH value of the electrolyte. However, to accurately interpret the E_d value, it is also important to consider that the local pH at the MnO_2/electrolyte interface can differ from the bulk and is indeed expected to rise significantly during the MnO_2 electrodissolution (according to the stoichiometry of reaction 1 and the unbuffered electrolyte used in the present study). Using eq. 2 and assuming that the process remains near thermodynamic equilibrium, the E_d value of 0.74 V translates into a local pH of ~3, thus slightly higher than the bulk pH 2. This agrees with a local conversion of acetic acid into acetate, which, as a function of their respective local activities and pK_a (4.74), determine the local pH according to the following modified Nernst equation:

$$E = E^0_{MnO_2/Mn^{2+}} - 0.12 \times pK_a + 0.12 \times \log\left(\frac{a_B}{a_{AH}}\right) - 0.03 \times \log\left(a_{Mn^{2+}}\right) \quad (3)$$

with a_{AH} and a_B the relative local activities of the AH weak acid and B conjugate base, respectively.

It is worth noting that at pH 2, the concentration of free protons (*i.e.*, H_3O^+, a stronger acid than acetic acid) remains too low (~10^{-2} M) to trigger the reductive electrodissolution of MnO_2. Indeed, discharging the MnO_2-GLAD-ITO electrode in a ~10 mM HCl electrolyte of pH 2, containing 2 M KCl and 0.1 M $MnCl_2$, results in a low capacity (linked to a poor *CE* of 40%) as well as a limited absorbance decrease (see Fig. 1C and 1D). At the end of this first discharge, the m_{MnO_2} value (quantified from XRF) indicates a residual MnO_2 amount as high as 60% of its initial value (Table S1), confirming that only partial electrodissolution occurs under these discharge conditions. Furthermore, we also note that the electrode potential decreases steadily during the discharge (no well-defined plateau), attesting to a local pH increase due to the significant depletion of H_3O^+ at the MnO_2/electrolyte interface. *On contrario*, at pH 1, the H_3O^+ concentration becomes sufficient (~0.1 M) to ensure full proton-coupled electrodissolution of MnO_2 (see Fig. 1C and 1D and Table S1). The discharge curve is quite similar to the one obtained in 1 M acetic acid electrolyte (*i.e.*, exhibiting a well-defined single discharge plateau with an almost 100% *CE*), except for the potential shift to more positive values resulting from the pH dependence of eq 2. As a consequence for further study, we deliberately avoided the overly concentrated Al^{3+}-based electrolytes (common in the literature) as they lead to very low pHs (Table S2) and thus to a dominant participation of H_3O^+ in the discharge process.

In Fig. 1A and 1B, the first galvanostatic discharges of MnO_2-GLAD-ITO electrodes in either 1 M $Al(OTf)_3$ or 1 M $AlCl_3$ aqueous electrolytes (pH 2) are overlaid in order to compare with the 1 M acetic acid (pH 2). The shapes and positions of the discharges as well as the absorption curves are almost identical to those recorded in the 1 M acetic acid, the only

difference being the appearance of a poorly-defined secondary discharge plateau, located at a lower potential. We do not believe these secondary plateaus are linked to aluminium ions in the electrolyte since they were previously observed in an Al^{3+}-free acidic electrolyte.[26] Alternatively, we suspect it could be related to nucleation and growth processes governing the electrodissolution of MnO_2, possibly because the latter becomes more difficult at the end of the discharge. For either Al^{3+}-based electrolyte, a full recovery of the electrode transparency was observed at the end of the discharge step (see pictures in Scheme 1), demonstrating full electrodissolution of MnO_2. This was also corroborated by both the high *CE* > 96% and the small m_{MnO_2} values at discharged electrodes (see Table S1). Accordingly, an exploitable gravimetric capacity as high as 550 $mA \cdot h \cdot g^{-1}$ could be achieved, almost identical to the value obtained in 1 M acetic acid. These observations lead to the irrefutable conclusion that we are again dealing with a two-electron MnO_2-to-Mn^{2+} conversion mechanism, involving protons (or proton donors) as the charge carriers. At this stage, the proton source in these Al^{3+}-based electrolytes remains an open question as we demonstrated above that the concentration of free protons at pH 2 could not trigger the electrodissolution process.

Another interesting feature of the discharge curves in Fig. 1A is their almost identical half-discharge potential values (Table S1), which indicates similar local pHs at the MnO_2/electrolyte interface, regardless of the nature of the electrolyte. On the basis of eq. 3, this implies that the proton donors involved in the MnO_2 conversion reactions are weak Brønsted acids of similar strength (*i.e.*, pK_a) as well as of similar activities. Given that the hexaaquo complex $[Al(H_2O)_6]^{3+}$ has a weak Brønsted acidity (pK_a = 4.9)[27] comparable to that of acetic acid (pK_a = 4.76) and that their concentrations are identical in both electrolytes, we can propose

the following proton-coupled MnO_2-reductive electrodissolution reaction in the Al^{3+}-based aqueous electrolytes:

$$Mn^{IV}O_2 + 4\,[Al(H_2O)_6]^{3+} + 4\,H_2O + 2\,e^- \rightarrow [Mn^{II}(H_2O)_6]^{2+} + 4\,[Al(H_2O)_5(OH)]^{2+} \quad (4)$$

This equation highlights the crucial role of $[Al(H_2O)_6]^{3+}$ as a proton donor to assist the conversion of MnO_2 at the metal oxide/electrolyte interface, which is here for the first time evidenced in the context of an electrodissolution mechanism. Given the limited pH increase occurring at the metal oxide/electrolyte interface during the discharge (*i.e.*, a local pH estimated to be 3 as discussed above), no precipitation of Al^{3+}-based hydroxides/oxides is observed in our spectroelectrochemical experiments, in contrast to what is reported in Zn^{2+}-based aqueous electrolytes.[28–30]

2.2. Cyclability in Al^{3+}-based electrolytes

Having shown that Al^{3+} triggers the efficient MnO_2 electrodissolution process during the discharge step, we next investigated the cyclability of the MnO_2-GLAD-ITO electrodes by spectroelectrochemistry. Once completely discharged, electrodes were subjected to galvanostatic cycling at a rate of 0.5 $mA \cdot cm^{-2}$, starting with a charge of 100 $mC \cdot cm^{-2}$. The data recorded at pH 2.0 in 1 M $Al(OTf)_3$ aqueous electrolyte containing 0.1 M $MnCl_2$ are reported in **Figure 2** (A to C, blue data). During the charging step, the potential rapidly stabilizes at 0.98 V while the absorbance of the electrode increases linearly (Fig. 2B), confirming a steady electrodeposition of MnO_2 to an amount close to that achieved for the electrodes loaded *ex situ*. The continuous galvanostatic cycling of the electrode demonstrates a remarkably stable and high *CE* (~97.5 % over 200 cycles, Fig. 2C), correlating well with the stable periodic electrode absorbance variations monitored during the first 25 cycles (Fig. 2B). In addition, apart from the secondary discharge plateau, which tends to progressively weaken, the galvanostatic charge/discharge

curves almost overlap during cycling. These results are consistent with a complete and highly reversible electrodeposition-electrodissolution process, without significant accumulation of MnO_2 or any other MnO_x material. It is worth noting that aluminium was below the limit of quantification in all the charged and discharged electrodes investigated by XRF. This confirms that the Al_xMnO_2 phase suggested in several works[14,15,17,18] is not formed, and also that the electrolyte is properly removed from the electrode material by thorough rinsing with water prior to *ex situ* analysis.

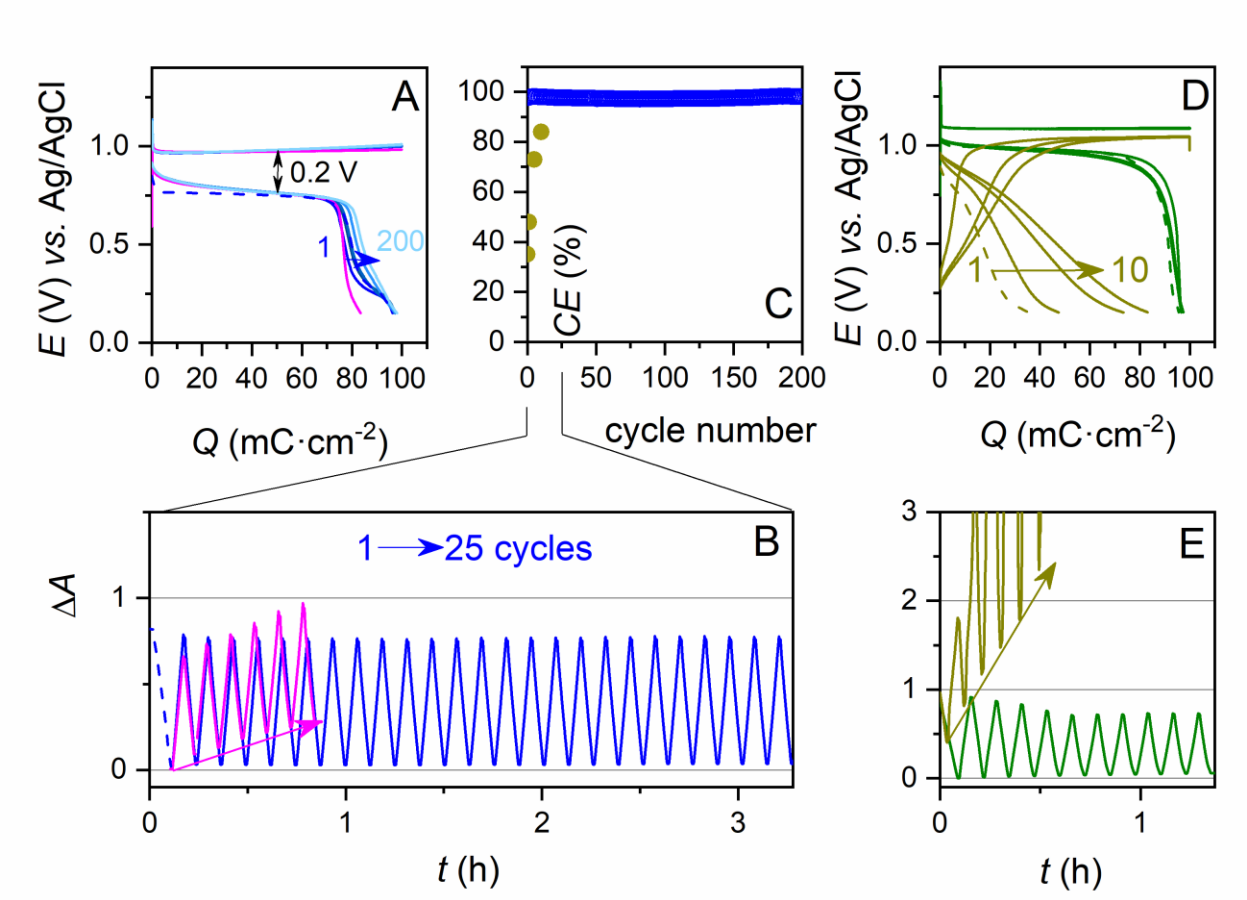

Figure 2. *In operando* spectroelectrochemical galvanostatic cycling of MnO_2-GLAD-ITO electrodes in different aqueous electrolytes. The first discharges (dashed lines) were performed at 0.3 mA·cm^{-2}, while the subsequent charge/discharge cycles (plain lines) were performed at 0.5 mA·cm^{-2}. (A) Galvanostatic charge/discharge curves and (B) concomitant absorbance variations,

as well as (C) associated Coulombic efficiencies (*CE*) recorded at GLAD-ITO electrodes cycled in Al^{3+}-based aqueous electrolytes made of either: (blue) 1 M $Al(OTf)_3$ + 0.1 M $MnCl_2$ (pH 2.0) or (magenta) 1.4 M $Al(OTf)_3$ + 7.1 mg/L MnO (pH 2.0) (see text for details). (D) Galvanostatic charge/discharge curves and (E) absorbance variations concomitantly recorded at a GLAD-ITO electrode cycled in an aqueous electrolyte containing 1 M KCl + 0.1 M $MnCl_2$ and with a pH adjusted to (dark yellow) 2.0 and (olive) 1.0. In D, the *in situ* cycles 1^{st}, 5^{th} and 10^{th} are shown (plain lines) and their corresponding *CE* are reported in C (dark yellow and olive dots).

The galvanostatic cycling experiments were also performed with MnO_2-GLAD-ITO electrodes in aqueous electrolytes adjusted with HCl to either pH 2.0 or pH 1.0 and containing 2 M KCl and 0.1 M $MnCl_2$ (Figs. 2D and 2E). As discussed above, after a first discharge in the electrolyte of pH 2.0, a significant amount of residual MnO_2 remains on the electrode surface. When the same electrode is then recharged to 100 $mC \cdot cm^{-2}$, the back electrodeposition of MnO_2 is well observed as attested by the absorbance increase (Fig. 2E). Given the stoichiometry of the electrodeposition reaction, the low *CE* of initial cycles is associated with a significant imbalance between proton consumption (during discharge) and release (during charge), thus leading to progressive acidification of the electrolyte with an increase of the *CE* during the subsequent cycles (Fig. 2C). Another consequence is the significant accumulation of MnO_2 at the electrode as evidenced by the continuous increase of the electrode absorbance with cycling up to saturation of the UV-vis spectrometer (Fig. 2E). *On contrario*, at pH 1, this electrolyte allows for a reversible electrodissolution/electrodeposition of a constant amount of MnO_2 without accumulation as shown by the relatively stable absorbance oscillation in Fig. 2E. This last behaviour is consistent with recent reports on rechargeable aqueous Zn/MnO_2 batteries operating in strongly acidic electrolytes.[26,31] The overall observations above definitely corroborate the crucial role played by the Al^{3+} hexaaquo complex as a weak Brønsted acid to trigger the

reversible electrodissolution of MnO_2 in aqueous electrolytes containing a low concentration of H_3O^+.

Owing to the conversion mechanism, the *in situ* electrodeposition of MnO_2 requires the presence of soluble Mn^{2+} ions in the electrolyte. This is commonly achieved by adding a highly soluble inorganic Mn^{2+} salt to the electrolyte. However, as shown below, it can also be achieved from a solid precursor such as MnO, calling into question the recent work of Yan *et al.* on the reversible insertion of Al^{3+} into MnO.[18] Indeed, in agreement with the Pourbaix diagram of manganese, it has been shown that MnO is prone to chemically dissolve in slightly acidic media.[32] To demonstrate that MnO can effectively dissolve in an Al^{3+}-based electrolyte and act as a soluble Mn^{2+} source, we replaced the initial Mn^{2+} salt by an equivalent amount of MnO in a 2 m $Al(OTf)_3$ electrolyte (*i.e.,* the same electrolyte used in ref. [18], see Experimental Section in Supporting Information). The resulting electrolyte was then used to cycle a fresh GLAD-ITO electrode. The results in Fig. 2A and 2B (magenta lines) show the successful electrodeposition/electrodissolution of MnO_2 under these conditions, thereby confirming the spontaneous chemical dissolution of MnO to Mn^{2+} in the Al^{3+}-based electrolyte. XRF analysis of the charged electrode indicates an electrodeposited m_{MnO_2} value of 44 $\mu g \cdot cm^{-2}$, comparable to that obtained with electrodes loaded *ex situ*. We were unable to discern aluminium in the XRF spectrum of the charged electrode, suggesting again the absence of an Al_xMnO_2 phase in contrast to what was previously reported.[18]

We next investigated the cyclability of the MnO_2-GLAD-ITO electrode in a two-electrode Zn/MnO_2 cell configuration (see Experimental Section in Supporting Information for details) with the electrolytes listed in Table S3 and containing Zn^{2+} to allow for the reversible Zn^{2+}-to-Zn conversion reaction at the anode. First, we verified that the addition of 0.25 M $ZnCl_2$

to the 1 M $AlCl_3$ + 0.1 M $MnCl_2$ electrolyte (pH 1.9) does not significantly affect the reversibility and efficiency of the MnO_2-to-Mn^{2+} conversion reaction. This was confirmed from the high *CE* of the galvanostatic cycles shown in **Figure 3** (A and C with corresponding data reported in Table S3) and the stable absorbance change recorded during cycling (Fig. 3B). Also in this electrolyte, the Zn/MnO_2 cell delivers an excellent and stable discharge gravimetric capacity of ~560 $mA \cdot h \cdot g_{MnO2}^{-1}$ over 100 cycles (one of the best gravimetric capacities reported so far for a Zn/MnO_2 cell). The cell also displays a remarkably high discharge voltage (~1.7 V) as well as an excellent energetic efficiency (*EE* > 80% at 10 $A \cdot g^{-1}$). The latter is the consequence of the low voltage hysteresis between the charge and discharge potentials, while the former is directly linked to the relatively low pH value of the electrolyte (*i.e.*, according to eq. 2 and considering that the Zn/Zn^{2+} couple is pH independent within the range of pHs investigated, the battery voltage is expected to gain 120 mV per pH unit decrease).

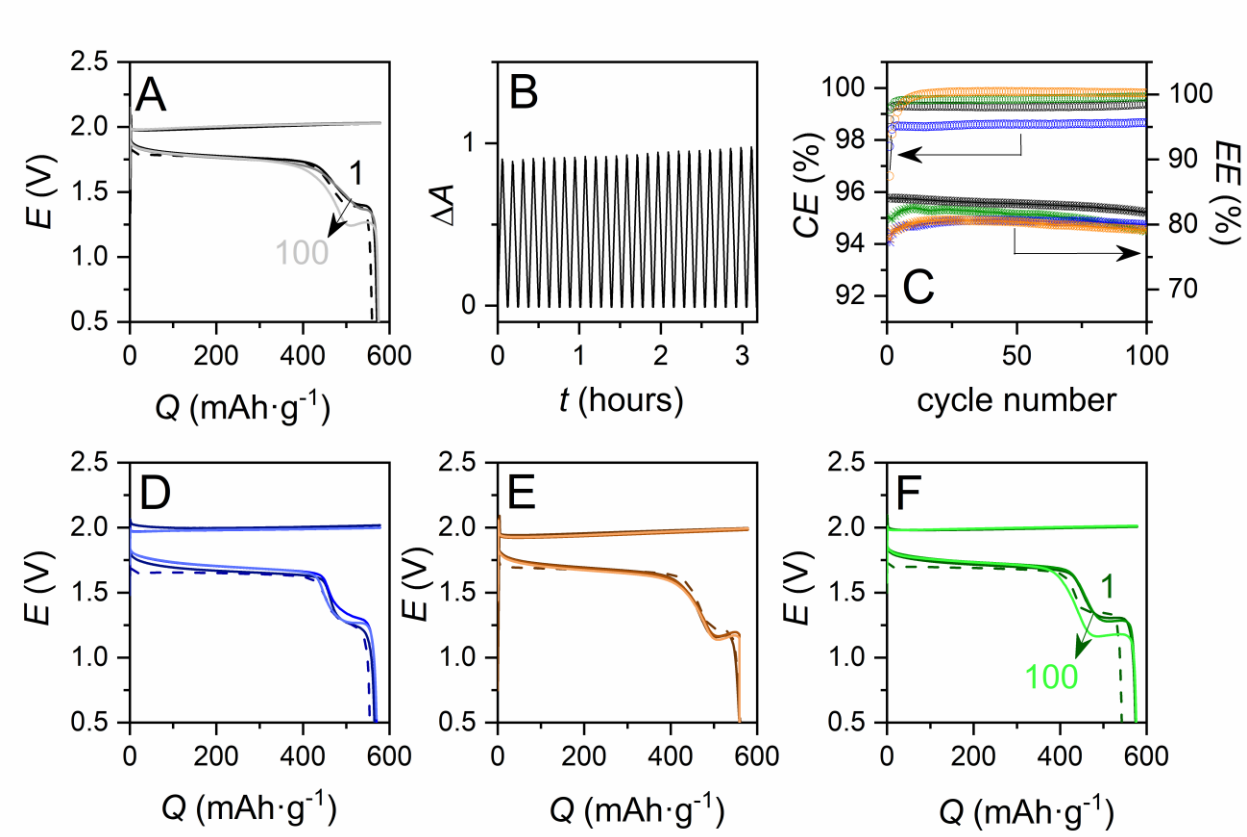

Figure 3. Galvanostatic cycles performed at a Zn foil/MnO_2-GLAD-ITO cell assembly (loaded *ex situ* with 48 $\mu g_{MnO2} \cdot cm^{-2}$) in the presence of the following Al^{3+}-based aqueous electrolytes: (A, B) 1 M $AlCl_3$ + 0.25 M $ZnCl_2$ + 0.1 M $MnCl_2$ (pH 1.90), (D) 1 M $Al(OTf)_3$ + 0.1 M $ZnCl_2$ + 0.1 M $MnCl_2$ (pH 1.77), (E) 1 m $Al(OTf)_3$ + 1 m $Zn(OTf)_3$ + 0.1 m $MnSO_4$ (pH 1.75), and (F) 1.25 M $Al(OTf)_3$ + 0.1 M $ZnCl_2$ + 0.1 M $MnCl_2$ (pH 1.5). The dashed black lines correspond to the 1st galvanostatic discharges (recorded at 0.3 $mA \cdot cm^{-2}$), while the solid lines are galvanostatic charge/discharge cycles (100 cycles at 0.5 $mA \cdot cm^{-2}$ with the 1st, 50th and 100th cycles shown). (C) Cycling performances of the Zn/MnO_2 cell assemblies mentioned in A to F (same color code).

The data presented in Fig. 3 and Table S3 show that the chemical composition of the Al^{3+}-based aqueous electrolytes has little effect on the shape and position of the galvanostatic charge/discharge curves. That all Zn/MnO_2 assemblies have such similar electrochemical

features indicates they share a common charge storage mechanism that we can attribute to the following dual reversible conversion process:

$$MnO_{2(s)} + 4\,[Al(H_2O)_6]^{3+} + Zn + 10\,H_2O \leftrightarrows [Mn(H_2O)_6]^{2+} + 4\,[Al(H_2O)_5(OH)]^{2+} + [Zn(H_2O)_6]^{2+} \quad (3)$$

This mechanism is further supported by the excellent gravimetric capacity we have systematically retrieved (*i.e.* > 550 $mA{\cdot}h{\cdot}g_{MnO2}^{-1}$), which interestingly is comparable to the value recently achieved in a strongly acidic electrolyte where the reversible proton-coupled conversion of MnO_2 into Mn^{2+} was fully established.[26]

We also tested the so-called bi-cation electrolyte (1 m $Al(OTf)_3$ + 1 m $Zn(OTf)_2$ + 0.1 m $MnSO_4$) used in ref [17]. Again, no significant change was observed in the charge/discharge curves (Fig. 3E), which confirms that the charge storage mechanism described above remains at work. This is in sharp contrast with the previously proposed mechanism based on the reversible co-insertion of H^+ and Zn^{2+} in an Al_xMnO_2 phase generated *in situ* (see further comment on pH considerations in the SI).[17] In such bi-cation electrolytes, the cyclability was actually improved with 100% capacity retention over 600 cycles (see Fig. S5 and **Table 1** - entry 1), demonstrating the high reversibility of the dual conversion process.

Table 1. Chemical composition and pH of the aqueous electrolytes used in Zn/MnO_x or Al/MnO_x assemblies and the main features of the galvanostatic cycling, *i.e.* rate ($A \cdot g^{-1}$), half-charge (E_c) and half-discharge (E_d) potentials (in V), maximal discharge capacity ($mA \cdot h \cdot g_{MnO2}^{-1}$), and Coulombic efficiency (*CE*).

electrolyte composition	pH	Anode	Rate	E_d	E_c	*CE*	Maximal discharge capacity	cathode mechanism	Ref
1 m $Al(OTf)_3$, 1 m $Zn(OTf)_3$, 0.1 m $MnSO_4$	1.75	Zn	10	1.65	1.95	99.7% over 600 cycles at 10 $A \cdot g^{-1}$	570	$MnO_2 \leftrightarrow Mn^{2+}$	This work
1.3 m $Al(OTf)_3$, 0.3 m $Zn(OTf)_3$, 0.3 m $MnCl_2$	1.74	Zn	2	1.65	1.84	99.5% over 1400 cycles at 2 $A \cdot g^{-1}$	560	$MnO_2 \leftrightarrow Mn^{2+}$	This work
1 M $ZnSO_4$, 1 M $MnSO_4$, 0.1 M H_2SO_4	1	Zn	0.58	1.95	2.2[b]	92% after 1800 cycles at 8.6 $A \cdot g^{-1}$	570	$MnO_2 \leftrightarrow Mn^{2+}$	[26]
1 M $Al(OTf)_3$, 1 M $Zn(OTf)_3$, 0.1 M $MnSO_4$	*ns*	Zn	0.1	~1.55	1.8	~100% over 1000 cycles at 1 C	264	Reversible co-insertion of Zn^{2+} and H^+ in Al_xMnO_2	[17]
2 M $Al(OTf)_3$	*ns*	Zn/Al alloy	0.1	1.6	1.8	~75% after 80 cycles at 0.1 $A \cdot g^{-1}$	460	$Al_xMnO_2 \leftrightarrow MnO$ with reversible uptake of Al^{3+}	[18]
2 m $Al(OTf)_3$, 0.1 m $Mn(OTf)_2$	*ns*	T-Al[a]	0.1	1.3	~1.6	~50% after 100 cycles at 0.2 $A \cdot g^{-1}$	310	$MnO_2 \leftrightarrow Mn_3O_4$	[13]
2 M $Al(OTf)_3$, 0.5 M $MnSO_4$	*ns*	T-Al[a]	0.1	1.3→1.15	1.6	~55% after 70 cycles at 0.1 $A \cdot g^{-1}$	554	$Al_xMn_{(1-x)}O_2 \leftrightarrow Mn^{2+}$	[15]
5 M $Al(OTf)_3$	< -0.5	Al	0.03	1.2 & 0.8	1.65	~60% after 65 cycles	467	Reversible Al^{3+} insertion in $Al_{x=0.1}MnO_2$	[14]

ns: not specified; [a] Aluminium anode pre-treated in an ionic liquid; [b] amperometric deposition.

Finally, to complete our demonstration of the universal character of the proposed mechanism, we have investigated a swagelock Zn/MnO_2 assembly in which electrospun carbon nanofibers (CNFs) loaded electrochemically with MnO_2[20] were used as the cathode (see Experimental Section in Supporting Information for details). Under these conditions, the active material mass versus electrolyte volume is increased by 2-orders of magnitude, thus making it more relevant to practical cell conditions. The CNFs were loaded with 0.5 mg·cm^{-2} MnO_2 (*i.e.*, 1 C·cm^{-2}) and further cycled in a 1.3 m $Al(OTf)_3$ + 0.3 m $Zn(OTf)_3$ + 0.3 m $MnCl_2$ electrolyte (pH 1.74). *Ex situ* SEM imaging of the cathode (Fig. S6) confirms the full electrodissolution of MnO_2 after the first discharge (*CE* = 97.8 % at 1 A·g^{-1}), as well as the back *in situ* electrodeposition of MnO_2 during the subsequent charge (1 C·cm^{-2}). With this cell assembly, an almost 100% capacity retention over 1400 cycles could be achieved at 2 A·g^{-1}, showing only a minor drift in the shape of the discharge ends as well as in the average charge/discharge voltage of the galvanostatic curves (Fig. S7). It is also worth noting that the half-charge and half-discharge potentials remain close to those recorded at the Zn/MnO_2-GLAD-ITO assembly (Table 1 – entry 2). These results thus show that MnO_2 electrodeposition/electrodissolution in Al^{3+}-based electrolytes does not depend on the nature of the conductive scaffold forming the cathode. It also demonstrates that the conversion mechanism we propose remains fully valid in a laboratory-scale battery.

2.3. Discussion

Overall, the present results shed new light on the aqueous aluminium batteries pairing a manganese oxide cathode with an aluminium or zinc anode,[13–18] for which the electrochemical features are gathered in Table 1. It is striking that cells based on identical anodes and electrolytes with similar pHs share such similar electrochemical features (notably charge/discharge potentials), thus suggesting thermodynamically equivalent electrochemical processes. Based on the present results, it is quite clear that MnO_x to Mn^{2+} conversion is a robust and invariable process independent of the nature of the cathode and/or Al^{3+}-based

electrolyte. In view of this behaviour, the diversity of mechanisms proposed in the literature (summarized in Table 1) raises questions, as it is very possible that a unified mechanism drives all the Al/MnO_x or Zn/MnO_x aqueous batteries gathered in Table 1.

One may however argue that complementary material characterization techniques are required to better probe our active material and to support the proposed unified charge storage mechanism. However, the characterization techniques based on *ex situ* or *in operando* spectroscopic analysis of the charged/discharged materials, such as XRD, XPS and elemental mapping analysis, are inconveniently blind to the dissolution processes and may mislead the interpretation of the charge storage mechanism. This is especially true for the reduced state Mn^{2+}, which once solubilised in the electrolyte, is no longer detectable by such techniques. Another difficulty is the amorphous state of the back electrogenerated MnO_x material, which unfortunately cannot be characterized by XRD. Despite this, several studies speculate on the *in situ* formation of a layered Al_xMnO_2 phase based on the detection of Al in the *ex situ* XPS spectra and energy dispersive spectroscopy mappings.[14,15,17,18] However, this is insufficient to irrefutably demonstrate the formation of an Al_xMnO_2 phase,[14,15,17,18] and to assert that Al^{3+} can reversibly insert into this phase.[14,18] It should be noted here that such *ex situ* analysis requires thorough rinsing of the composite electrodes in order to get rid of the concentrated electrolyte that is trapped inside.[15]

Another important aspect that is often improperly considered is that the cyclability of the Zn/MnO_2 batteries improves when sufficient Mn^{2+} (0.1 to 0.5 M) is added into the Al^{3+}-based electrolytes.[13,15,17] Rather than inhibiting or suppressing the dissolution of Mn^{2+}, we and other groups demonstrated that the role of pre-added Mn^{2+} in the aqueous electrolytes is to act as a reservoir for MnO_2 electrodeposition during charging.[12,29,33] This is the principle of a conversion battery, where finally the capacity of the electrolyte has to be taken into account for the energy density calculation.

Some publications report on lower oxidation state manganese oxide cathode materials (*i.e.*, spinel Mn_3O_4 and MnO) capable of cycling in highly concentrated $Al(OTf)_3$ aqueous electrolytes, free of Mn^{2+} ions.[14,18] The problem with such oxides is that they tend to spontaneously dissolve in acidic electrolytes,[32,34] as we have shown here with MnO. Because of the rather high concentration of $Al(OTf)_3$ used in these studies (> 2 M at pH < 0, see Table S2), Mn^{2+} is expected to be generated *in situ* from the spontaneous chemical dissolution of the Mn_3O_4- or MnO-based cathode. After a certain time, a significant amount of Mn^{2+} is thus present in these electrolytes, fulfilling the requirements for a reversible MnO_2-to-Mn^{2+} conversion.

Finally, some authors suggest the reversible insertion of multivalent cations (Al^{3+} or Zn^{2+}) in an *in situ* activated layered phase of Al_xMnO_2.[14,17] The present study clearly demonstrates that neither Al^{3+} nor Zn^{2+} can reversibly insert in the active MnO_x phase, the latter being entirely dismantled by the proton-coupled electrodissolution process.

3. Conclusion

The present study unambiguously demonstrates that the reversible proton-coupled MnO_2-to-Mn^{2+} conversion is the main charge storage mechanism of MnO_x-based cathodes when cycled in Al^{3+}-based aqueous electrolytes. By avoiding excessively high concentrations of Al^{3+} ions associated with strongly acidic conditions, we highlighted the essential role of the $[Al(H_2O)_6]^{3+}$ complex as a proton donor, allowing exploitation of the 2-electron charge storage capacity of MnO_2 with high cyclability and efficiency. The nature of the counter ions has little effect over the charge storage, making MnO_2-to-Mn^{2+} conversion a robust mechanism that was likely unknowingly involved in previous studies.

Supporting Information

Experimental Section, Supplementary Figs. S1 to S7, and Tables S1 to S3 and additional comments. Supporting Information is available from the Wiley Online Library.

Acknowledgements

The authors thank Ivonne Cocca and Sophie Nowak (Université de Paris) for X-ray fluorescence measurements. We also gratefully acknowledge financial support from the French National Agency (ANR AqReBat project).

References

[1] J. Shin, J. W. Choi, *Adv. Energy Mater.* **2020**, 2001386.

[2] D. Chao, W. Zhou, F. Xie, C. Ye, H. Li, M. Jaroniec, S. Qiao, *Sci. Adv.* **2020**, *6*, eaba4098.

[3] M. J. Park, H. Y. Asl, A. Manthiram, *ACS Energy Lett.* **2020**, *5*, 2367.

[4] Z. Rong, R. Malik, P. Canepa, G. Sai Gautam, M. Liu, A. Jain, K. Persson, G. Ceder, *Chem. Mater.* **2015**, *27*, 6016.

[5] V. Mathew, B. Sambandam, S. Kim, S. Kim, S. Park, S. Lee, M. H. Alfaruqi, V. Soundharrajan, S. Islam, D. Y. Putro, J. Hwang, Y. Sun, J. Kim, *ACS Energy Lett.* **2020**, *5*, 2376.

[6] W. Manalastas, S. Kumar, V. Verma, L. Zhang, D. Yuan, *ChemSusChem* **2019**, *12*, 379.

[7] T. Liu, X. Cheng, H. Yu, H. Zhu, N. Peng, R. Zheng, *Energy Storage Mater.* **2019**, *18*, 68.

[8] Z. Li, S. Ganapathy, Y. Xu, Z. Zhou, M. Sarilar, M. Wagemaker, *Adv. Energy Mater.* **2019**, *1900237*, 1.

[9] Q. Zhao, L. Liu, J. Yin, J. Zheng, D. Zhang, J. Chen, L. Archer, *Angew. Chemie Int. Ed.* **2020**, *59*, 1.

[10] M. J. Park, A. Manthiram, *ACS Appl. Energy Mater.* **2020**, *3*, 5015.

[11] Y.-S. Kim, K. D. Harris, B. Limoges, V. Balland, *Chem. Sci.* **2019**, *10*, 8752.

[12] M. Mateos, N. Makivic, Y.-S. Kim, B. Limoges, V. Balland, *Adv. Energy Mater.* **2020**, *10*, 2000332.

[13] Q. Zhao, M. J. Zachman, W. I. Al Sadat, J. Zheng, L. F. Kourkoutis, L. Archer, *Sci. Adv.* **2018**, *4*, eaau8131.

[14] C. Wu, S. Gu, Q. Zhang, Y. Bai, M. Li, Y. Yuan, H. Wang, X. Liu, Y. Yuan, N. Zhu, F. Wu, H. Li, L. Gu, J. Lu, *Nat. Commun.* **2019**, *10*, 73.

[15] S. He, J. Wang, X. Zhang, J. Chen, Z. Wang, T. Yang, Z. Liu, Y. Liang, B. Wang, S.

Liu, L. Zhang, J. Huang, J. Huang, L. A. O. Dell, H. Yu, *Adv. Funct. Mater.* **2019**, 1905228.

[16] J. Joseph, J. Nerkar, C. Tang, A. Du, A. P. O'Mullane, K. Ostrikov, *ChemSusChem* **2019**, *12*, 3753.

[17] N. Li, G. Li, C. Li, H. Yang, G. Qin, X. Sun, F. Li, H. Cheng, *ACS Appl. Mater. Interfaces* **2020**, *12*, 13790.

[18] C. Yan, C. Lv, L. Wang, W. Cui, L. Zhang, K. N. Dinh, H. Tan, C. Wu, T. Wu, Y. Ren, J. Chen, Z. Liu, M. Srinivasan, X. Rui, *J. Am. Chem. Soc.* **2020**, *142*, 15295615304.

[19] M. Mateos, K. D. Harris, B. Limoges, V. Balland, *ACS Appl. Energy Mater.* **2020**, *3*, 7610.

[20] A. Singh, O. Sel, H. Perrot, V. Balland, B. Limoges, C. Laberty-Robert, *J. Mater. Chem. A* **2021**, Advance Article.

[21] K. M. Krause, M. T. Taschuk, K. D. Harris, D. A. Rider, N. G. Wakefield, J. C. Sit, J. M. Buriak, M. Thommes, M. J. Brett, *Langmuir* **2010**, *26*, 4368.

[22] H. Pan, Y. Shao, P. Yan, Y. Cheng, K. S. Han, Z. Nie, C. Wang, J. Yang, X. Li, P. Bhattacharya, K. T. Mueller, J. Liu, *Nat. Energy* **2016**, *1*, 16039.

[23] A. J. Bard, R. Parsons, J. Jordan, Eds. , *Standard Potentials in Aqueous Solution*, CRC Press, **1985**.

[24] M. Huynh, D. K. Bediako, Y. Liu, D. G. Nocera, *J. Phys. Chem. C* **2014**, *118*, 17142.

[25] C. Costentin, D. G. Nocera, *J. Phys. Chem. C* **2019**, *123*, 1966.

[26] D. Chao, W. Zhou, C. Ye, Q. Zhang, Y. Chen, L. Gu, K. Davey, S. Z. Qiao, *Angew. Chemie - Int. Ed.* **2019**, 7823.

[27] D. R. Lide, Ed. , *CRC Hanbook of Chemistry and Physics*, CRC Press, Bocan Raton, FL, **2005**.

[28] B. Lee, H. R. Seo, H. R. Lee, C. S. Yoon, J. H. Kim, K. Y. Chung, B. W. Cho, S. H. Oh, *ChemSusChem* **2016**, *9*, 2948.

[29] J. Yang, J. Cao, Y. Peng, W. Yang, S. Barg, Z. Liu, I. A. Kinloch, M. A. Bisset, R. A. W. Dryfe, *ChemSusChem* **2020**, *13*, 4103.

[30] C. F. Bischoff, S. Fitz, J. Burns, M. Bauer, H. Gentischer, K. P. Birke, H. Henning, D. Biro, *J. Electrochem. Soc.* **2020**, *167*, 020545.

[31] W. Chen, G. Li, A. Pei, Y. Li, L. Liao, H. Wang, J. Wan, Z. Liang, G. Chen, H. Zhang, J. Wang, Y. Cui, *Nat. Energy* **2018**, *3*, 428.

[32] C. F. Jones, R. St, C. Smart, P. S. Turner, *J. Chem. Soc. Faraday Trans.* **1990**, *86*, 947.

[33] D. Wu, L. M. Housel, J. Kim, N. Sadique, C. D. Quilty, L. Wu, R. Tappero, S. L. Nicholas, S. Ehrlich, Y. Zhu, A. C. Marschilok, E. S. Takeuchi, D. C. Bock, K. J. Takeuchi, *Energy Environ. Sci.* **2020**, *13*, 4322.

[34] I. V. Artamonova, I. G. Gorichev, E. B. Godunov, *Engineering* **2013**, *05*, 714.